RSC Advances

COMMUNICATION

View Article Online
View Journal | View Issue

Cite this: *RSC Adv.*, 2015, **5**, 40907

Received 17th March 2015
Accepted 10th April 2015

DOI: 10.1039/c5ra04671h

www.rsc.org/advances

Using an "underwater superoleophobic pattern" to make a liquid lens array

Jiale Yong, Qing Yang, Feng Chen,* Guangqing Du, Chao Shan, Umar Farooq, Jiuhong Wang and Xun Hou

This paper reports a new strategy to realize real liquid lens arrays without evaporation problems based on an underwater superoleophobic–oleophobic heterogeneous pattern. The flat circular region shows an inherent underwater oleophobicity while the femtosecond laser ablated region displays underwater superoleophobicity. In a water medium, the oil droplet is restricted to the untreated circle by the energy barrier at the superoleophobic–oleophobic boundary, thereby forming a convex lens shape by surface tension. The liquid lens array benefits from the surrounding water and then overcomes the problem of evaporation. The shape of the liquid lens can be simply controlled by the designed pattern and the oil volume.

1 Introduction

The lens is a common optical device and it is widely applied in optical communication, microscopy, light convergence/divergence, photography, laser microfabrication, and so on.[1–5] Many methods have been developed to form various lenses, including machining,[6] thermal reflow,[7] hot embossing,[8] the droplet method,[9] two-photon polymerization,[10,11] and femtosecond laser wet etching.[12,13] Among these techniques, liquid lenses have attracted considerable attention because of the simple process, economical material, and the easy adjustment of the focal length.[14–16] This method relies on the surface tension of a liquid droplet, such as water, to form a part-sphere shape which can be used as a convex lens. However, some defects limit the wide applications of liquid lenses. Evaporation is the most frequently mentioned disadvantage, which results in the shape of the lens being unstable because the volume decreases with time.[17] To avoid this problem, a liquid polymer (for example, hydrogels and sol–gels) is used instead of water.[18,19] The liquid polymer is solidified as soon as the lens shape of the polymeric droplet forms. As a result, the lens does not suffer from evaporation, but it is at the solid state. This lens is not a "real" liquid lens although its formation is based on the property of the liquid polymer. On the other hand, liquid lenses need to keep enough distance from each other when preparing a lens array; otherwise they will easily mix together. The liquid lens array is usually not aligned orderly due the location of the liquid lenses being difficult to control. Therefore, there is still a great challenge ahead in fabricating a real uniform liquid lens array without evaporation.

Here, the glass surface is selectively ablated by a femtosecond laser to form an array pattern of circles, which is composed of bare flat circles with a surrounding laser-induced microstructure. The laser ablated and untreated regions respectively show underwater superoleophobicity and ordinary weak oleophobicity. The difference in wettability generates an energy barrier, which can restrict the oil droplet on the untreated circle. The oil droplet with a part-spherical shape and the surrounding water form a converging lens.

2 Experimental

Fig. 1 depicts the fabrication procedure of the non-evaporating liquid lens schematically. We started by forming a pattern composed of an array of bare flat untreated array of circles with a surrounding laser-induced region, using selective femtosecond laser ablation (Fig. 1a and b). The diameter of the circle, D, and the size of each unit, L, can be arbitrarily designed. The experimental setup and femtosecond laser ablated method were shown in our previous work.[20–22] The glass sample was fixed on a computer controlled translation stage. The laser beam (wavelength = 800 nm; pulse duration = 50 fs; repetition rate = 1 kHz) was focused on the glass surface *via* an objective lens (NA = 0.45, Nikon). During the line-by-line scanning process, the laser power, scanning speed, and the interval of scanning lines were set at 20 mW, 2 mm s^{-1}, and 2 μm, respectively. A mechanical shutter was used to turn the femtosecond laser

State Key Laboratory for Manufacturing System Engineering & Key Laboratory of Photonics Technology for Information of Shaanxi Province, School of Electronics & Information Engineering, Xi'an Jiaotong University, Xi'an, 710049, P. R. China. E-mail: chenfeng@mail.xjtu.edu.cn

beam on and off. After the pattern was fabricated and cleaned, the as-prepared sample was immersed into water. The water was treated in advance to meet the limit of solubility of the oil (chloroform), although chloroform is very difficult to dissolve in water (chloroform : water = 1 mL : 200 mL). Then, a small oil droplet hanging from a microsyringe was lowered down by a micromechanical system and contacted with the untreated flat circle. Increasing the volume of oil made the three-phase contact line (TPCL) advance until it reached the boundary of the laser-induced and untreated domains. As it was difficult to ensure whether the TPCL fully overlapped with the edge of untreated circle, an oil droplet with an excess volume was placed on the flat circle in our experiment. Next, the redundant oil was sucked up until the residual amount reached the designed value (Fig. 1c). During this process, the TPCL did not shrink for the contact angle hysteresis although the oil volume decreased continuously.

3 Results and discussion

Fig. 2a is a digital photo of the as-prepared surface which is composed of a periodic untreated uniform circle array (6 × 4) and a rough laser-induced region. There is a sharp boundary between the untreated and the laser-induced domains (Fig. 2b and c). The femtosecond laser ablated region is characterized by rough ridges with the size of several micrometers, decorated with abundant nano-particles with the diameter of just a few tens of nanometers (Fig. 2d). The surface roughness (S_a) is about 0.667 μm. The clear boundary between the laser ablated and the untreated regions, as well as the femtosecond laser-induced rough microstructure, is also demonstrated by its three-dimensional (3D) and cross-sectional profiles, obtained using a laser confocal scanning microscope, as shown in Fig. 3. The micro/nanometer binary structures play a key role in achieving the underwater superoleophobicity. Fig. 2e reveals the image of an oil droplet on the completely rough surface in the water medium. The oil droplet keeps a spherical shape, and the oil contact angle (OCA) can reach up to 160.5° ± 2°. In addition, it is very difficult to land the oil droplet on the femtosecond laser ablated surface. The oil droplet will roll off if the substrate is tilted only 1°, demonstrating an ultralow oil-adhesion in water (Fig. 2f). Compared with the laser ablated domain, the untreated region has an inherent weak underwater oleophobicity with an OCA of 121° ± 3°. Therefore, the array pattern of circles is composed of underwater superoleophobic and ordinary oleophobic domains, giving a heterogeneous topography.

The glass shows an inherent hydrophilicity in the air, while its wettability can be significantly enhanced to superhydrophilicity

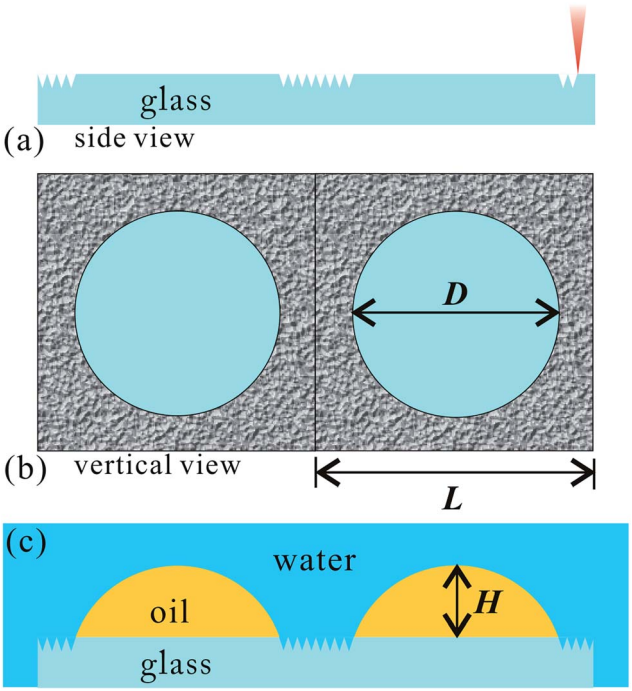

Fig. 1 Schematic diagram of the formation process for the liquid lens array. (a and b) Side and vertical views of the fabrication of an array pattern composed of bare flat circles and a surrounding rough microstructure formed by femtosecond laser selective ablation. (c) Placing the fabricated sample into water and dropping oil droplets onto the bare flat circles.

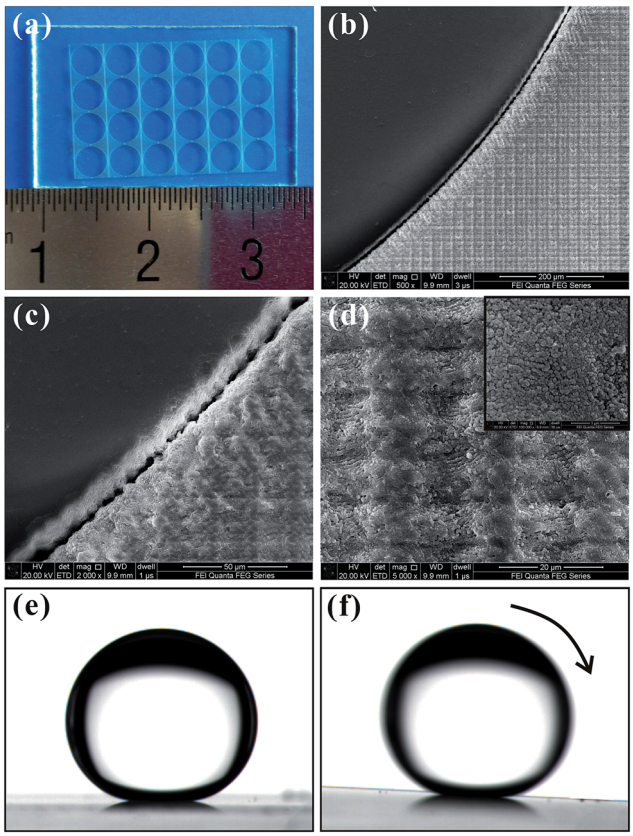

Fig. 2 (a) Digital image of the as-prepared array pattern of circles, composed of untreated circles and a rough laser induced region. (b and c) SEM images with different magnifications of the boundary between the untreated and femtosecond laser ablated regions. (d) SEM images of the femtosecond laser ablated glass surface. (e) A 8 μL oil droplet on the completely femtosecond laser ablated surface. (f) Oil droplet rolling off the completely femtosecond laser ablated surface tilted by 1°.

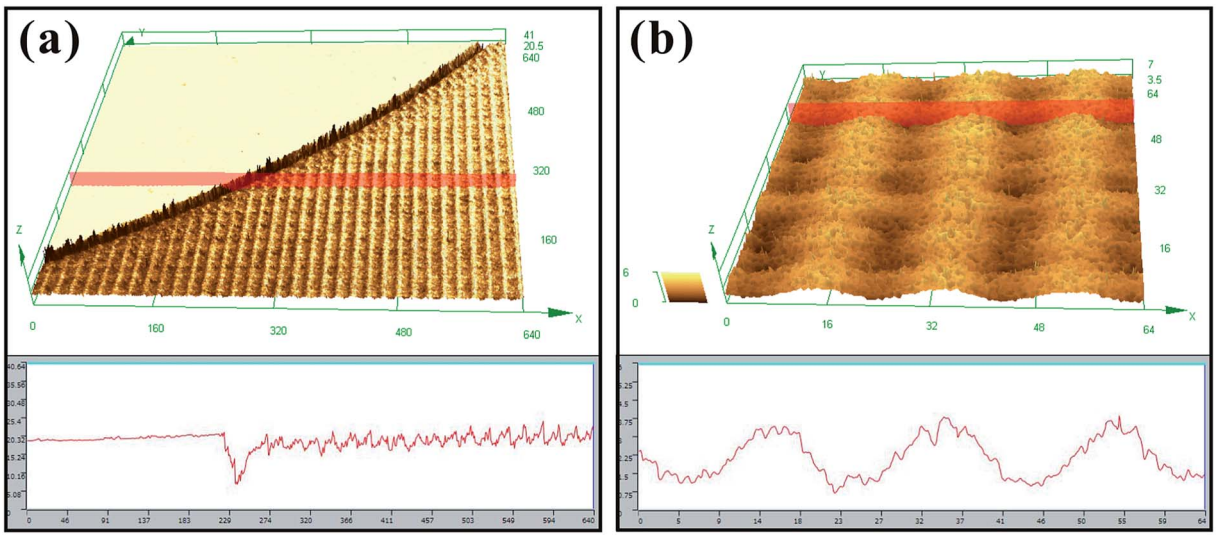

Fig. 3 3D images and cross-sectional profiles of the as-prepared pattern. (a) Boundary at laser ablated and non-ablated regions: ×400. (b) Femtosecond laser-induced microstructure: ×4000.

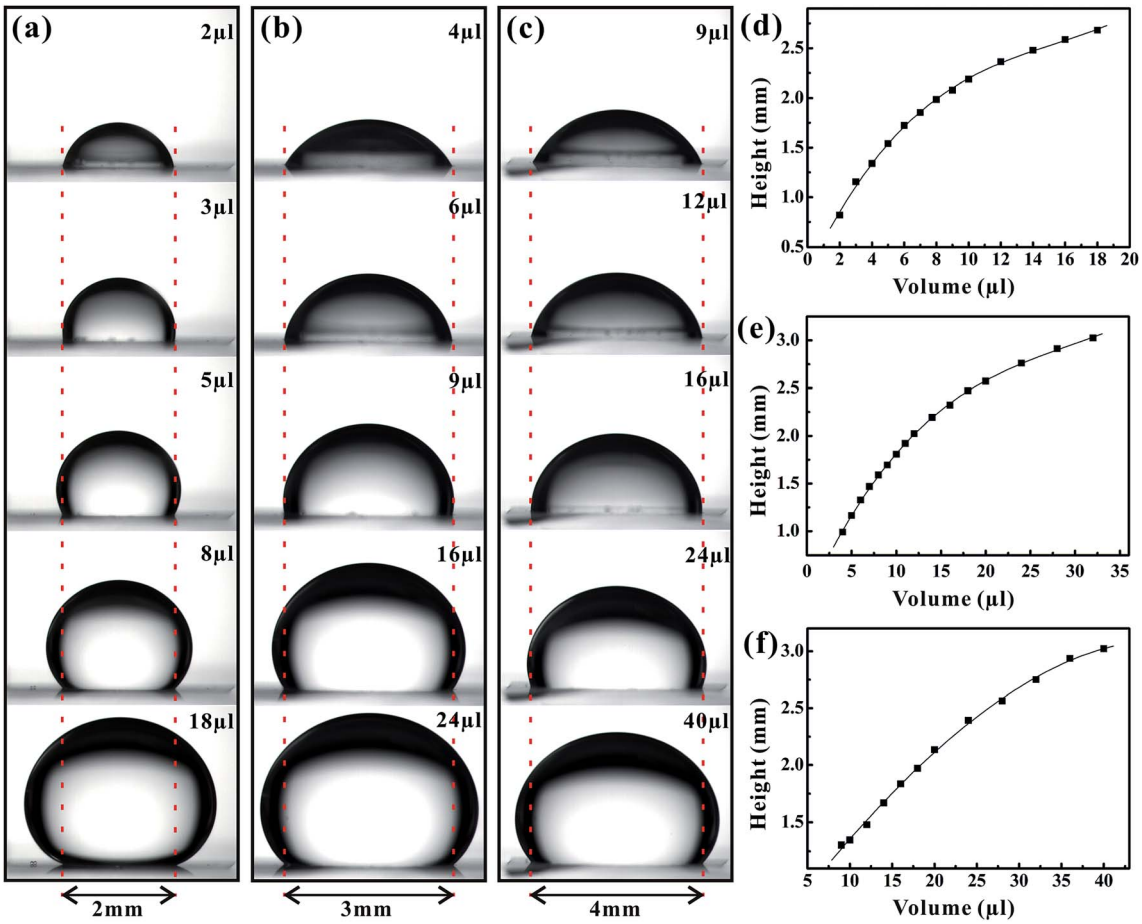

Fig. 4 The controllable shape of the as-prepared liquid lens by designing the diameter of the circle and the oil volume. (a–c) Shapes of underwater oil droplets with different volumes on the circle patterns: (a) $D = 2$ mm, (b) $D = 3$ mm, (c) $D = 4$ mm. (d–f) Relationship between the height of the lens and the volume of the underwater oil droplets: (d) $D = 2$ mm, (e) $D = 3$ mm, (f) $D = 4$ mm.

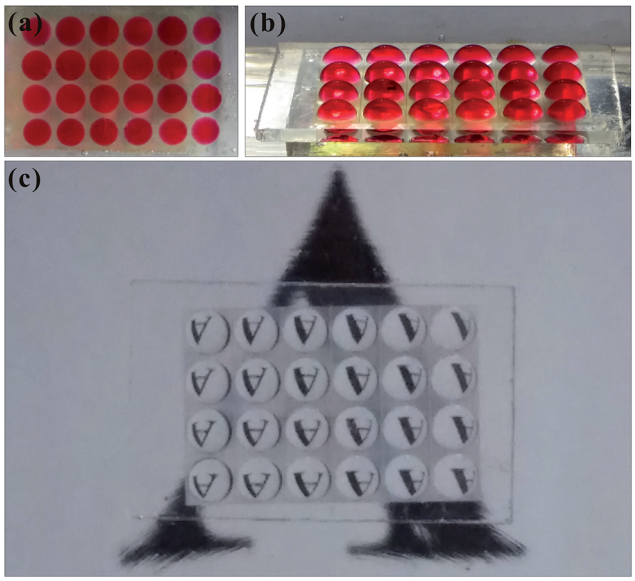

Fig. 5 (a and b) Vertical and side views of the liquid lens array. For observation, the oil was dyed with Sudan III, thereby showing a red color. (c) Image of an object after passing through the as-prepared liquid lens array.

by femtosecond laser ablation due to the rough microstructure formation.[23] Water will immediately enter into the interspaces of the laser-induced rough microstructure as soon as the sample is immersed in water, forming a water cushion between the oil droplet and the sample. This trapped water layer endows the oil droplet with the ability of sitting only on the top of the microstructure. Such a three-phase system (oil/water/solid) is usually described by the underwater version of Cassie's model.[24,25] Here, the high OCA can be explained by the following equation:

$$\cos\theta^{*}_{\mathrm{ow}} = \lambda\cos\theta_{\mathrm{ow}} + \lambda - 1 \tag{1}$$

where θ^{*}_{ow} and θ_{ow} are the contact angle of an oil droplet on the laser ablated surface and the bare flat glass surface in the water medium, respectively. λ is the area fraction of the projected oil wet area. Accordingly, λ can be calculated to be 0.04 in our experiment. This small value reveals that the underwater oil droplet only contacts a small area of the femtosecond laser ablated rough surface. The trapped water cushion is an ideal oil-repellent material for the repulsive interaction between the nonpolar (oil) and polar (water) molecules, endowing the femtosecond laser ablated region with underwater superoleophobicity.[26]

In general, an energy barrier can form at the boundary between the different chemical domains or with morphologies with different apparent surface free energies.[27–32] Oil droplets can stick to the bare flat glass surface, which shows ordinary oleophobicity in water, even when the substrate is tilted 90° or 180°, representing a steady state. On the contrary, the underwater oil droplet on the laser ablated glass surface is at an unstable state because the surface displays underwater superoleophobicity and the oil droplet can roll off easily by a slight disturbance. The steady and unstable states indicate that the object is in the low and highest energy cases, respectively. Based on the Gibbs' criterion, an energy barrier that needs to be overcome exists in the process of the oil droplet spreading across from the flat untreated circle to the laser-induced rough region.[27,28] By gradually increasing the volume of the oil droplet, the oil droplet first contacts the flat untreated domain and generates a strong attraction; meanwhile, the edge of the oil droplet advances until it reaches the boundary between the untreated and the laser-induced regions. Then, the energy barrier will prevent the oil droplet moving forward, even with the oil volume continuing increasing. As a result, the underwater oil droplet is restricted to the untreated circle by the energy barrier at the boundary between the untreated underwater ordinary oleophobic and underwater superoleophobic laser-induced regions, thereby forming a part-sphere shape from the surface tension. This two-phase system, including the part-sphere oil and the surrounding water, can act as liquid lens.

The shape of the as-prepared liquid lens can be easily controlled by the designed diameter of the circle and the oil volume. Fig. 4a–c show the shapes of an underwater oil droplet on the circle pattern. It can be seen that the oil droplet is restricted on bare flat regions, keeping a partial sphere shape. With the volume increasing, the droplet becomes bigger, while the contact area between the oil droplet and glass substrate remains constant. For every fabricated sample, the height (H) of the lens increases with the gradual increasing of the oil volume (Fig. 4d–f). According to our operational process of pushing away and then sucking up the oil, the range of the contact angle of the oil lens is from the receding contact angle (~56°) of the oil droplet on a flat glass surface to the advancing contact angle (~160.5°) of the oil droplet on the laser-induced rough substrate. Combining the different diameters and oil volumes, various optical parameters for the liquid lens can be obtained. The controllability makes the application of the fabricated liquid lens more flexible and convenient. Interestingly, the underwater oil lens is very stable, and its shape has almost no change after one week of storage. This happens because the oil droplet is immersed in water and thereby avoids evaporation, unlike water droplets that exist in the air. The feature of non-evaporation endows the liquid lens with long-term applications.

Fig. 5a and b show digital photos of the as-prepared lens array with $D = 3$ mm, $L = 3.2$ mm, and oil volume = 6 μL. The H was computed to 1.33 mm based on the shape of the side image (Fig. 4b). The oil lenses are uniformly arranged and located very close to each other. There is no need to worry that the lenses will mix together due to the good isolation effect of the femtosecond laser ablated region. Since the refractive index of water is smaller than that of chloroform, the as-prepared liquid lens composing of a part-sphere oil droplet and the surrounding water medium is a converging lens. The typical optical parameters of the liquid lens array (radius of curvature, R, focal length, f, and numerical aperture, NA) can be estimated by the following equations:[33,34]

$$R = \frac{(D/2)^2 + H^2}{2H}, \quad f = \frac{n_{\mathrm{w}}R}{n_{\mathrm{o}} - n_{\mathrm{w}}}, \quad \mathrm{NA} = \frac{D}{2f} \tag{2}$$

where n_w is the refractive index of water, and n_o is the refractive index of the oil (chloroform). For example, the lenses shown in Fig. 5 have $D = 3$ mm, $H = 1.33$ mm, $n_w = 1.33$, and $n_o = 1.45$. The R, f, and NA of those lenses are calculated as 1.51 mm, 16.74 mm, and 0.09, respectively. The imaging ability was tested by placing a paper with a black letter "A" below the lens plane. The distance between the lens array and the object was about 20 cm. An array of inverted real images was clearly observed by the camera above the lenses, as shown in Fig. 5c. The excellent readability of the letters reflects the good imaging property and the uniformity of the liquid lens array.

4 Conclusions

In conclusion, a kind of real and uniform liquid lens array without an evaporation problem was realized by an oil-water two-phase system. The glass surface is selectively ablated by a femtosecond laser to form an array pattern of circles, composed of bare flat circles and a surrounding laser-induced microstructure, which show inherent underwater oleophobicity and superoleophobicity, respectively. In a water medium, the oil droplet is restricted to the untreated circle by the energy barrier at the boundary of the underwater superoleophobic–oleophobic heterogeneous regions, thereby forming a convex lens shape by surface tension. The as-prepared liquid lens array does not have the problem of evaporation because the oil droplet is in a water medium. In addition, the shape of the liquid lens can be controlled by the designed diameter of the circle and the oil volume. This paper is only a proof-of-concept. In the future, the impact of the thickness of the surrounding water, as well as the packaging technology, needs be further investigated. The aperture of the lens will hopefully be reduced to smaller than 1 mm as the technology becomes more accomplished.

Acknowledgements

This work is supported by the National Science Foundation of China under Grant nos 51335008, 61275008, and 61176113, the Special-funded programme on national key scientific instruments and equipment development of China under the Grant no. 2012YQ12004706, and the Collaborative Innovation Center of high-end Manufacturing equipment. The SEM work was done at the International Center for Dielectric Research (ICDR), Xi'an Jiaotong University; we greatly appreciate Juan Feng's help for obtaining the SEM images.

References

1 Y. L. Sun, W. F. Dong, R. Z. Yang, X. Meng, L. Zhang, Q. D. Chen and H. B. Sun, *Angew. Chem., Int. Ed.*, 2012, **51**, 1558.
2 X. Li, Y. Ding, J. Shao, H. Tian and H. Liu, *Adv. Mater.*, 2012, **24**, OP165.
3 F. Chen, Z. Deng, Q. Yang, H. Bian, G. Du, J. Si and X. Hou, *Opt. Lett.*, 2014, **39**, 606.
4 X. H. Lee, I. Moreno and C. C. Sun, *Opt. Express*, 2013, **21**, 10612.
5 D. X. Lu, Y. L. Zhang, D. D. Han, H. Wang, H. Xia, Q. D. Chen, H. Ding and H. B. Sun, *J. Mater. Chem. C*, 2015, **3**, 1751.
6 A. Y. Yi and L. Li, *Opt. Lett.*, 2005, **30**, 1707.
7 H. Yang, C. K. Chao, M. K. Wei and C. P. Lin, *J. Micromech. Microeng.*, 2004, **14**, 1197.
8 N. S. Ong, Y. H. Koh and Y. Q. Fu, *Microelectron. Eng.*, 2002, **60**, 365.
9 L. Dong, A. K. Agarwal, D. J. Beebe and H. Jiang, *Nature*, 2006, **442**, 551.
10 D. Wu, S. Z. Wu, L. G. Niu, Q. D. Chen, R. Wang, J. F. Song, H. H. Fang and H. B. Sun, *Appl. Phys. Lett.*, 2010, **97**, 031109.
11 D. Wu, J. N. Wang, L. G. Niu, X. L. Zhang, S. Z. Wu, Q. D. Chen, L. P. Lee and H. B. Sun, *Adv. Opt. Mater.*, 2014, **2**, 751.
12 H. Liu, F. Cheng, Q. Yang, P. Qu, S. He, X. Wang, J. Si and X. Hou, *Appl. Phys. Lett.*, 2012, **100**, 133701.
13 F. Chen, H. Liu, Q. Yang, X. Wang, C. Hou, H. Bian, W. Liang, J. Si and X. Hou, *Opt. Express*, 2010, **18**, 20334.
14 C. Li and H. Jiang, *Appl. Phys. Lett.*, 2012, **100**, 231105.
15 A. O. Ashtiani and H. Jiang, *Appl. Phys. Lett.*, 2013, **103**, 111101.
16 Y. S. Lu, H. Tu, Y. Xu and H. Jiang, *Appl. Phys. Lett.*, 2013, **103**, 261113.
17 D. Kang, C. Pang, S. M. Kim, H. S. Cho, H. S. Um, Y. W. Choi and K. Y. Suh, *Adv. Mater.*, 2012, **24**, 1709.
18 Z. Ding and B. Ziaie, *Appl. Phys. Lett.*, 2009, **94**, 081111.
19 X. Jin, D. Guerrero, R. Klukas and J. F. Holzman, *Appl. Phys. Lett.*, 2014, **105**, 031102.
20 J. Yong, F. Chen, Q. Yang, G. Du, C. Shan, H. Bian, U. Farooq and X. Hou, *J. Mater. Chem. A*, 2015, **3**, 9379.
21 J. Yong, F. Chen, Q. Yang, D. Zhang, G. Du, J. Si, F. Yun and X. Hou, *J. Phys. Chem. C*, 2013, **117**, 24907.
22 D. Zhang, F. Chen, Q. Yang, J. Yong, H. Bian, Y. Ou, J. Si, X. Meng and X. Hou, *ACS Appl. Mater. Interfaces*, 2012, **4**, 4905.
23 J. Yong, F. Chen, Q. Yang, D. Zhang, U. Farooq, G. Du and X. Hou, *J. Mater. Chem. A*, 2014, **2**, 8790.
24 M. Liu, S. Wang, Z. Wei, Y. Song and L. Jiang, *Adv. Mater.*, 2009, **21**, 665.
25 J. Yong, Q. Yang, F. Chen, H. Bian, G. Du, U. Farooq and X. Hou, *Adv. Mater. Interfaces*, 2015, **2**, 1400388.
26 Q. Wen, J. Di, L. Jiang, J. Yu and R. Xu, *Chem. Sci.*, 2013, **4**, 541.
27 J. Yong, F. Chen, Q. Yang, U. Farooq, H. Bian, G. Du and X. Hou, *Appl. Phys. Lett.*, 2014, **105**, 071608.
28 J. Yong, Q. Yang, F. Chen, D. Zhang, U. Farooq, G. Du and X. Hou, *J. Mater. Chem. A*, 2014, **2**, 5499.
29 L. Tie, Z. Guo and W. Li, *RSC Adv.*, 2015, **5**, 8446.
30 W. Li and A. Amirfazli, *J. Colloid Interface Sci.*, 2005, **292**, 195.
31 W. Li and A. Amirfazhi, *Adv. Colloid Interface Sci.*, 2007, **132**, 51.
32 L. Tie, Z. Guo and W. Li, *J. Colloid Interface Sci.*, 2014, **436**, 19.
33 J. Yong, F. Chen, Q. Yang, G. Du, H. Bian, D. Zhang, J. Si, F. Yun and X. Hou, *ACS Appl. Mater. Interface*, 2014, **5**, 9382.
34 B. Hao, H. Liu, F. Chen, Q. Yang, P. Qu, G. Du, J. Si, X. Wang and X. Hou, *Opt. Express*, 2012, **20**, 12939.